ELSEVIER

Contents lists available at ScienceDirect

Optics and Lasers in Engineering

journal homepage: www.elsevier.com/locate/optlaseng



Keyhole cutting of carbon fiber reinforced polymer using a long-duration nanosecond pulse laser



Timothy Heiderscheit^a, Ninggang Shen^a, Qinghua Wang^a, Avik Samanta^a, Benxin Wu^b, Hongtao Ding^{a,*}

- ^a Department of Mechanical and Industrial Engineering, University of Iowa, Iowa City, IA 52242, United States
- ^b School of Mechanical Engineering, Purdue University, West Lafayette, IN 47907, United States

ARTICLE INFO

Keywords: Laser cutting Carbon fiber reinforced polymer Keyhole Long pulse Nanosecond pulse laser

ABSTRACT

The machining performance of a high-energy nanosecond pulse laser with a near-infrared wavelength is investigated for carbon fiber-reinforced polymer (CFRP) with two different fiber arrangements. This research work demonstrates for the first time that a keyhole mode cutting can be achieved for CFRP materials using a high-energy nanosecond pulse laser of a Long Pulse mode (120 ns). Specifically, it is shown that the short-duration Q-Switch mode (8 ns) results in ineffective material removal for CFRP, despite much higher peak laser power intensity than the Long Pulse mode. In Long Pulse mode, multi-pass straight line and contour cutting experiments are further performed to investigate the effect of laser processing parameters and resultant machined surface integrity. Plasma absorption effects using both pulse modes are discussed. The results show that a 2.2 mm thick cross-ply CFRP panel can be cut through using as few as 6 laser passes, and a high-quality machined surface can be produced with a limited heat-affected zone and minimal fiber pull-out using Argon assist gas. The successful outcomes from this work provide the key to enable efficient CFRP laser machining using high-energy nanosecond pulse lasers, and offer insight into the unique energy absorption mechanisms for CFRP laser machining.

1. Introduction

Non-contact laser machining is becoming a viable solution for high-speed machining of carbon fiber-reinforced polymer (CFRP) without the detrimental effects of mechanical cutting force and tool degradation. Laser machining of CFRP is defined as an ablation process, where the fiber-matrix structure is directly removed from the substrate by photon absorption. Although there has been a significant study on laser source options and the effect of individual process parameters in the literature, there is potential for further investigation into specific material removal and energy absorption mechanisms using a long-duration nanosecond pulse laser at a near-infrared (NIR) wavelength.

A wide range of laser source options have been investigated by researchers. Salama et al. [1,2] employed a transversely-excited atmospheric-pressure (TEA) $\rm CO_2$ laser for machining of CFRP. Their tests showed minimal thermal damage, likely from increased matrix absorption at a wavelength of 10.6 μ m. However, $\rm CO_2$ lasers generate large spot diameters that produce wide kerfs, reduce power intensity, and limit the ablation rate. Jung et al. [3] evaluated laser machining using a 1030 nm CW disk laser for both long- and short-fiber CFRP. Their tests showed a significant heat-affected zone (HAZ) expansion due to contin-

uous laser-material interaction, and a subsequent reduction in tensile strength during high power and low scanning speed conditions. Leone et al. [4] analyzed the CFRP removal mechanism and HAZ formation using a Q-Switched Yb:YAG fiber laser working at a pulse duration of 50 ns with low pulse energy (0.2–1.0 mJ). Li et al. [5] investigated laser machining quality with a Nd:YVO₄ and claimed a HAZ width of only 50 μ m using 25 ns pulses. Mathew et al. [6] performed CFRP machining experiments using a high-energy Nd:YAG laser system. Relatively long pulse duration in the range of 0.2–1.0 ms produced widespread matrix recession and charring in their study.

Good machining results have been achieved using ultraviolet laser (UV) lasers. Anzai et al. [7] concluded by comparing trepanning performance using a prototype dual-beam scanning system with a CW singlemode NIR fiber laser and an ns-pulsed UV laser. Similarly, Fujita et al. [8] compared different combinations of pulse duration (fs to ns) and wavelength (266 nm to 1064 nm). Takahashi et al. [9] directly compared CFRP laser machining at 266 nm and 1064 nm with a Q-Switched Nd:YAG laser, and concluded that matrix absorptivity was a key factor in determining machined surface integrity. The matrix material is largely transparent in the NIR spectrum. Therefore, laser irradiation passes through the matrix and is absorbed by the fibers, indirectly heating the matrix by conduction and causing fiber pull-out and HAZ extension.

E-mail address: hongtao-ding@uiowa.edu (H. Ding).

Corresponding author.

Table 1Properties for Hexcel HexTow[®] fibers [24,25].

Property	HexTow® IM7 (for cross-ply CFRP)	HexTow® AS4 (for woven CFRP)
Fiber diameter (μm)	5.2	7.1
Carbon content (%)	95	94
Tensile strength (MPa)	5515–5655	4410-4620
Failure elongation (%)	1.9	1.7-1.8
Conductivity (W/m·K)	5.4	6.8
Specific heat (J/kg·K)	879	1130
Mass density (kg/m ³⁾	1780	1790

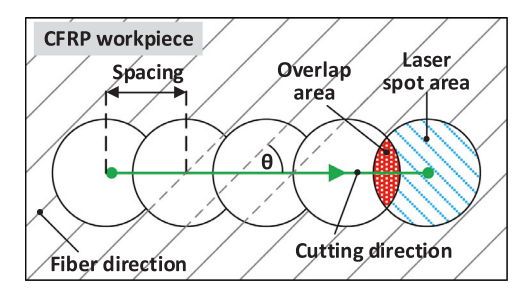


Fig. 1. Schematic of laser scan path over CFRP workpiece during nanosecond laser machining experiments. Scan path direction, θ , is relevant for cross-ply samples only.

Conversely, UV irradiation is absorbed by the matrix directly. Wolynski et al. [10] investigated three laser wavelengths (355 nm, 532 nm, 1064 nm) to estimate the ablation threshold by extrapolating measurements for ablated width over a range of laser fluences. The calculated threshold increased with wavelength, with the volumetric ablation rate also being 25% lower for 355 nm than for 1064 nm. Given the transparency of the CFRP matrix for the NIR spectrum, it was postulated that the penetration depth of the laser irradiation would be greater since a portion of UV laser energy is absorbed by the matrix according to Beer's Law.

Due to the thermal nature of the process, traditional surface roughness metrics are insufficient to quantify CFRP laser machined surface quality. Analysis of surface integrity using SEM imaging is important beyond HAZ formation at the workpiece surface. Voisey et al. [11] analyzed fiber swelling during laser percussion drilling of CFRP using a 1.06 µm Nd:YAG laser system. SEM imaging revealed radial swelling as high as 60% for fibers near the drilled wall. They used Raman spectroscopy to conclude that removing impurities through the use of heattreated T300 PAN-based fibers reduced fiber swelling. It is also possible that the swelling mechanism was the result of inelastic thermal expansion from energy absorption due to the high pulse energy (1.0 J) over long pulse duration (1.0 ms). Fuchs et al. [12] noted a similar effect using a continuous-wave NIR Yb:YAG fiber. Fiber ends near at the wall surface swelled and combined with re-solidified matrix material to become fused. Similarly, matrix recession near the internal wall surface was observed during NIR laser machining [9]. Theoretically, this could lead to cracking and compromise the fatigue life of the CFRP structure. Li et al. [13] analyzed the CFRP microstructure for multi-ring laser drilling using a high power Q-Switched Nd:YVO4 DPSS UV laser system and also saw evidence of "cracking" and voids in the local fiber-matrix structure. The multi-ring scanning technique led to heavily-modified surface integrity along the multi-ring profiles.

It is generally agreed that the use of inert assist gases in CFRP laser machining reduces thermal damage by limiting exothermic oxidation reactions, while reactive gases promote fiber-matrix decomposition and enhance the material removal process. Riveiro et al. [14] improved the CO₂ laser cutting process for CFRP by using an Argon assist gas flow to decrease the heat-affected zone (HAZ) width. Rodden [15] conducted laser drilling experiments using a NIR Nd:YAG laser with long pulse

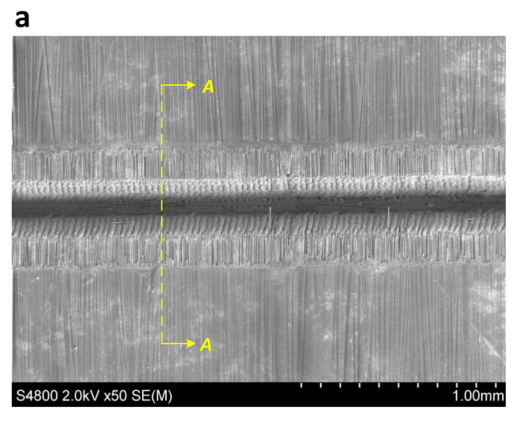
duration of 0.1 ms to illustrate the effect of inert assist gas on plasma formation and reduced HAZ expansion. Negarestani et al. [16] similarly evaluated the effect of mixed reactive and inert assist gases for laser cutting of CFRP using a nanosecond-pulsed Nd:YAG laser. Both studies observed enhanced machining performance in the presence of oxygen or reactive gas environments. French et al. [17] compared $\rm N_2$ and $\rm CO_2$ assist gases using a long duration (0.3–0.5 ms) laser system at high pulse energy (1.8 J to 6.0 J). They hypothesized the Joule-Thompson effect was responsible for improved drilling quality with less surface debris using $\rm CO_2$ assist gas.

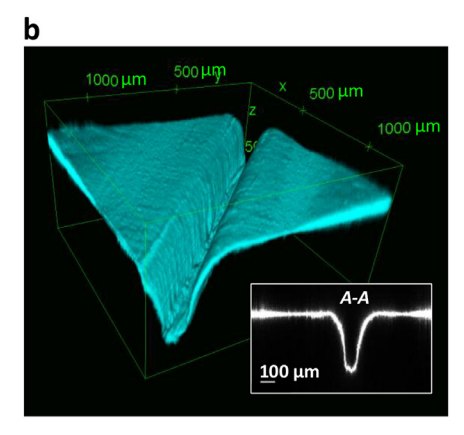
Ultra-fast pulsed laser scanning has been shown to improve CFRP machining quality. High performance laser drilling of CFRP using a highfrequency picosecond NIR laser system was demonstrated [1]. Thermal damage was significantly reduced, but at the expense of processing time. As many as 500 laser passes were required to drill through a 2 mm thick CFRP sample using a multi-ring strategy, with a 6 mm sample requiring a half hour of processing time. This is likely due to the low ablation rate (~15 nm/pulse) that is typical of ultrafast-pulsed laser systems as a result of low pulse energy (< 1 mJ). Similarly, experiments by Finger et al. [18] showed very high CFRP machining quality with ${<}5\,\mu m$ HAZ on 2 mm thick samples using an 80 W picosecond laser at an ablation rate of 100 mm³/min. The primary advantage of ultra-fast pulsed laser scanning for CFRP is that the short duration is less than the thermal response time of the substrate. Loumena et al. [19] reduced the HAZ by at least a factor of 5 by deploying femtosecond-pulsed processing versus nanosecond-pulsed at fluences higher than 3 J/cm². Finding a way to deliver high pulse energy over a short pulse duration represents the ultimate goal for CFRP laser processing: delivering high machining quality with acceptable processing times.

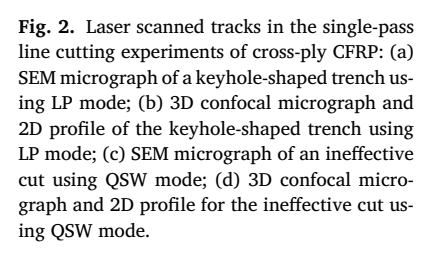
Researchers have attempted to correlate the laser ablation rate to process parameters in an attempt to measure the ablation threshold, but some inconsistent results have been reported. Wolynski et al. [10] estimated the threshold fluence of CFRP to be approximately $0.410\,\mathrm{J/cm^2}$ for $1064\,\mathrm{nm}$ wavelength using $10\,\mathrm{ps}$ pulses by extrapolating the ablated width. Hoffman et al. [20] proposed a slightly higher estimate of $0.52\,\mathrm{J/cm^2}$ for graphite using longer $10\,\mathrm{ns}$ pulses, also at a wavelength of $1064\,\mathrm{nm}$, by extrapolating the observed ablation rate. Lednev et al. [21] reported the laser ablation threshold of carbon nanotubes to be only $50\,\mathrm{mJ/cm^2}$ using a nearly identical $1064\,\mathrm{nm}$ laser. As such, the exact relationship between the CFRP ablation rate and laser irradiance is not clear. An alternative for characterizing laser materials processing was originally proposed by Beal et al. [22] and applied to the CFRP laser machining process by Romoli et al. [23]. Energy density is a measure of total laser energy delivered to a laser scanned area (Eq. (1)).

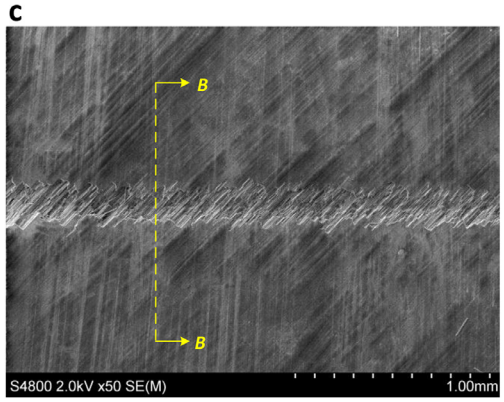
$$ED \left[J/mm^2 \right] = \frac{P_{avg}}{v \cdot d} \tag{1}$$

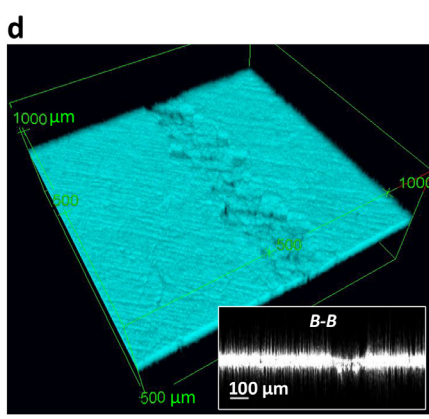
All relevant pulse and scanning properties are accounted for, with average laser power, P_{avg} , laser scanning speed, ν , and laser spot diameter, d. Traditional parameters, such as laser fluence and power density, quantify pulse energy or peak laser power delivered per unit area, respectively. Using a high-frequency Q-Switched Nd:YAG UV laser, Romoli et al. [23] calculated the threshold energy density of Toray T300 fibers to be $0.58\,\mathrm{J/mm^2}$, two orders of magnitude lower than threshold fluence estimates. Energy density has not been used extensively in











studying laser machining of CFRP, and offers flexibility to compare laser systems over a wide range of process parameters.

Laser machining of CFRP using a high-energy laser source has not been well studied in the literature, especially for high-energy long-duration nanosecond pulsing at low frequency. In this study, the performance of a high-energy nanosecond laser is experimentally evaluated for single-pass or multi-pass line cutting and contour machining of cross-ply CFRP. This is in contrast to previous research discussed above regarding low-power ultra-fast laser processing of CFRP. In particular, the physiochemical nature of the material removal and energy absorption mechanisms is addressed. The effects of process parameters are evaluated for single-pass line cutting using both cross-ply and woven CFRP. Surface integrity analysis is carried out for through cuts obtained by multi-pass line cutting and contour cutting.

2. Experiments

Two CFRP materials were used in this study: (1) cross-ply IM7 $12\,\mathrm{K}$ fiber-reinforced polymer with ${\sim}62\%$ fiber volume fraction and (2) woven 5HS AS4 $6\,\mathrm{K}$ fiber-reinforced polymer with 57% fiber volume fraction. Both fiber types are manufactured by Hexcel Corporation using CYCOM® 977–3 epoxy resin system for primary and secondary aerospace structure applications, with high impact resistance under both hot and wet conditions. The sample thickness was $2.2\,\mathrm{mm}$ for both CFRP materials. Other properties for the carbon fibers are listed in Table 1.

Laser beam machining experiments were conducted for carbon fiber-reinforced polymers using a high-energy Nd:YAG nanosecond pulsed laser system (Quanta-Ray[®] Lab-150, 1064 nm, 10 Hz) with a Gaussian distribution profile. Laser scanning was implemented using an intelliS-can scan head and controlled using ScanLab computer software. An argon assist gas flow was sprayed over the target area to evacuate debris, aid workpiece cooling, and prevent oxidization. The average power was calculated by the laser pulse energy and repetition rate. In this study,

the applied maximum average power was about 3 W, i.e., the applied maximum pulse energy was about 300 mJ.

Fig. 1 shows the typical laser scan path for line cutting experiments. The spacing defines the distance between two sequential laser pulses along the scanning direction, and is determined by the laser repetition rate, f, and preset laser scanning speed, ν . The overlap ratio (OR, %) represents the ratio of overlap area from consecutive pulses to the laser spot area as shown in Fig. 1. For the cross-ply IM7 CFRP, the scan path direction relative to fiber orientation in the top layer was defined by the angle θ as shown in Fig. 1.

During single-pass laser line cutting experiments, two different pulse modes were evaluated: Q-Switch (QSW) and Long Pulse (LP), which generate a short-duration laser pulse of 8 ns and a long-duration laser pulse of 120 ns, respectively. Cutting performance was evaluated for both cross-ply and woven CFRP specimens over a range of energy density levels. Performance was defined by the width of the matrix evaporation zone (MEZ), kerf width, and cutting depth. For cross-ply CFRP, the effects of cutting direction were examined by comparing performance for parallel ($\theta=0^\circ$) and orthogonal ($\theta=90^\circ$) fiber orientations relative to the cutting direction. In contour cutting experiments, 4 mm and 6 mm diameter circular holes were drilled using a standard trepanning scanning technique.

Surface analysis was performed after laser cutting experiments using a scanning electronic microscope (SEM) (Hitachi, S-4800). The kerf and MEZ width were measured on the SEM micrographs. In this work, the heat-affected zone was mainly characterized using the MEZ measurement. Three-dimensional (3D) surface profiles of line cuts were characterized using a confocal microscopy system (Zeiss, LSM 710) equipped with a 488 nm argon laser illumination source. To measure the depth of cut, two-dimensional (2D) surface profiles were obtained by slicing the 3D confocal microscope surface profile using an open source software package (ImageJ).

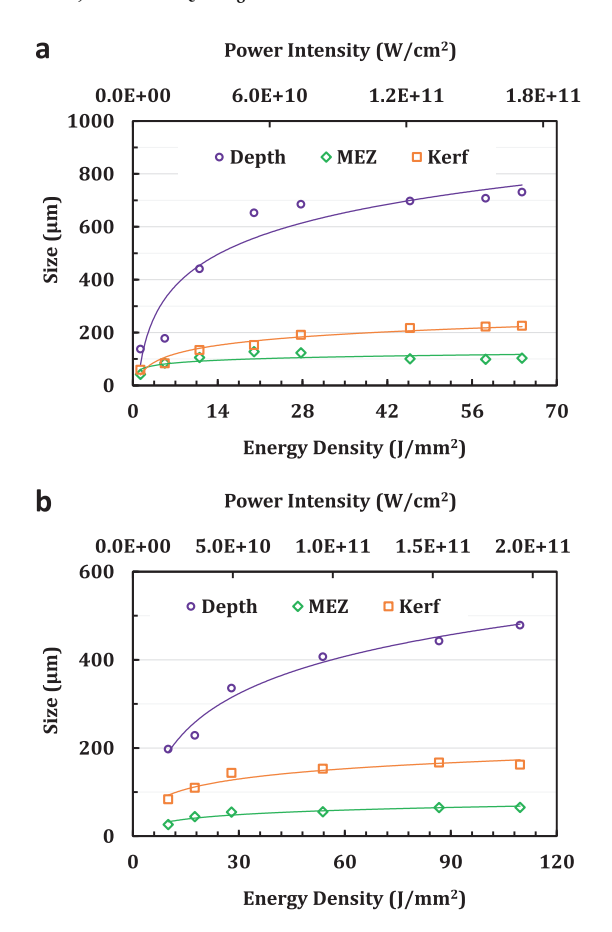


Fig. 3. The effects of laser power in single-pass laser line cutting using LP mode for: (a) cross-ply IM7 CFRP ($d = 40 \,\mu\text{m}$, OR = 0%); (b) woven AS4 CFRP ($d = 75 \,\mu\text{m}$, OR = 47%).

3. Results and discussions

3.1. LP mode vs. QSW mode

Fig. 2 shows the SEM and confocal micrographs of the typical surface morphology for cross-ply CFRP after a single laser scan in LP and QSW mode. Fig. 2a shows a single-pass laser scan in LP mode produced a clean cut with very minor defects using a spot size of 200 µm under laser power intensity of 2.8×10^9 W/cm². In this article, laser power intensity refers to peak intensity unless otherwise noted. The 3D surface profile of the cut was obtained using the confocal microscope, which was a deep cut as shown in Fig. 2b. The 3D confocal micrograph was sectioned using ImageJ software to obtain the 2D cross-sectional surface profile. The cross-sectional micrograph shows a clean trench profile with a keyhole shape, and the kerf and depth of cut were $230\,\mu m$ and 367 µm, respectively. As shown in Fig. 2c, no significant cut was obtained after a single-pass laser scan in Q-Switch mode using a spot size of 40 μm under a power intensity of 6.0×10^{10} W/cm². From Fig. 2d, the matrix resin was partially removed along the scanned path, with fibers at the top surface of the CFRP specimen cut at a negligible depth. The 2D cross-sectional surface profile shows limited change in surface profile that was less than the signal noise on the adjacent uncut surface. No trench could be formed by increasing the power intensity (as high as $1.3 \times 10^{12} \, \text{W/cm}^2$), with only a greater area of matrix resin being removed. QSW mode was deemed ineffective, even though the laser power intensity was many orders of magnitude greater than that of LP mode.

The drastic difference in cutting performance is attributed to the fundamental change of laser-material interaction at high power intensity. A hypothesized explanation will be given next for the different performances of laser cutting using LP mode or QSW mode. In this study, the power intensity for QSW experiments ranged from 5.5×10^{10} W/cm² to $1.3 \times 10^{12} \,\mathrm{W/cm^2}$, which is high enough to exceed the capability of linear optical absorption. This range is also significantly higher than typical power intensity values from prior studies, which generally use low-energy nanosecond lasers below 5 GW/cm², similar to Takahashi et al. and Sato et al. [26,27]. Optical breakdown of the gas environment above the target area might occur at sufficiently high power intensity. This threshold intensity was experimentally measured using a Nd:YAG laser with 6 ns pulses based on the multiphoton ionization theory [28]. The threshold was inversely proportional to wavelength with the optical breakdown for 1064 nm wavelength occurring above approximately 4.42 GW/cm² [29]. This threshold is inversely proportional to pulse duration, with energy from longer pulses being dissipated before optical breakdown can occur. Based on this estimate, the power intensity of the high-energy laser employed in this study in QSW mode was sufficient to cause optical breakdown and create a plasma plume around the CFRP top surface. The laser-induced material breakdown could lead to the generation of plasma consisting of ionized argon and/or ionized target material. The formed plasma would be highly absorptive, and prevent a significant portion of the pulse energy from reaching the CFRP top surface. Previous work has measured absorption of the incident photon energy for such conditions to be as high as 80%, attributed to the inverse Bremsstrahlung mechanism by Sankaranarayanan and Kar [30] and Morgan [31]. As a result, the laser beam cannot penetrate beyond the CFRP target surface at such a reduced intensity. Therefore, material removal in QSW mode, using a minimum intensity of 5.5×10^{10} W/cm², can only occur near the target surface and only a shallow cutting depth is produced.

During initial testing, parameters from QSW mode were repeated in LP mode, with the only variable being pulse duration. For the same pulse energy, laser power intensity is higher in QSW mode due to the shorter duration given the fixed laser frequency of 10 Hz. The results confirmed the above observations regarding the ineffectiveness of Q-Switch mode due to exceeding the ionization threshold of the air environment. LP mode can successfully machine CFRP due to power intensity being less than the threshold for 1064 nm wavelength and 120 ns pulse duration. Additionally, the high end of the power intensity range tested in LP mode overlaps with the low end the range of power intensity tested in OSW mode. Peak laser power is calculated by dividing the measured average laser power and dividing by duration and frequency. Dividing again by spot area yields the laser power intensity. Therefore, it can be deduced that the pulse duration at least partially determines the ionization threshold. The physiochemical dependence on laser pulse duration and wavelength of this mechanism is beyond the scope of this study. Exceeding the optical breakdown threshold during laser machining of CFRP has been similarly observed in other research. Intense photon absorption by laser-induced plasma as a result of optical breakdown was observed in experiments using 10 ns pulses at an intensity of 3×10^9 W/cm² in a standard air environment [32]. Optical breakdown was subsequently avoided using 200 ns pulses at a reduced intensity of 1.5×10^8 W/cm².

Results using Long Pulse demonstrated unique keyhole mode laser material removal. Keyhole laser cutting is usually achieved for metal alloys using continuous-wave (CW) lasers, e.g., CO_2 laser cutting of mild steels. Preissig et al. [33] summarized that the keyhole is usually caused by vapor pressure due to the intense laser irradiation and multiple laser ray reflections in those processes. The local vapor pressure creates, deepens, and maintains the expanded keyhole during laser cutting. The keyhole mode laser cutting of metals can be more efficient than classical laser cutting techniques, because the melt can be removed much more efficiently from the center line in the cut front. This makes the melt film thinner to ensure efficient heat conduction from the melt surface. However, the molten material film is unlikely to be developed in this study due to the limited energy input over a short duration for a nanosecond pulse laser compared with a CW laser.

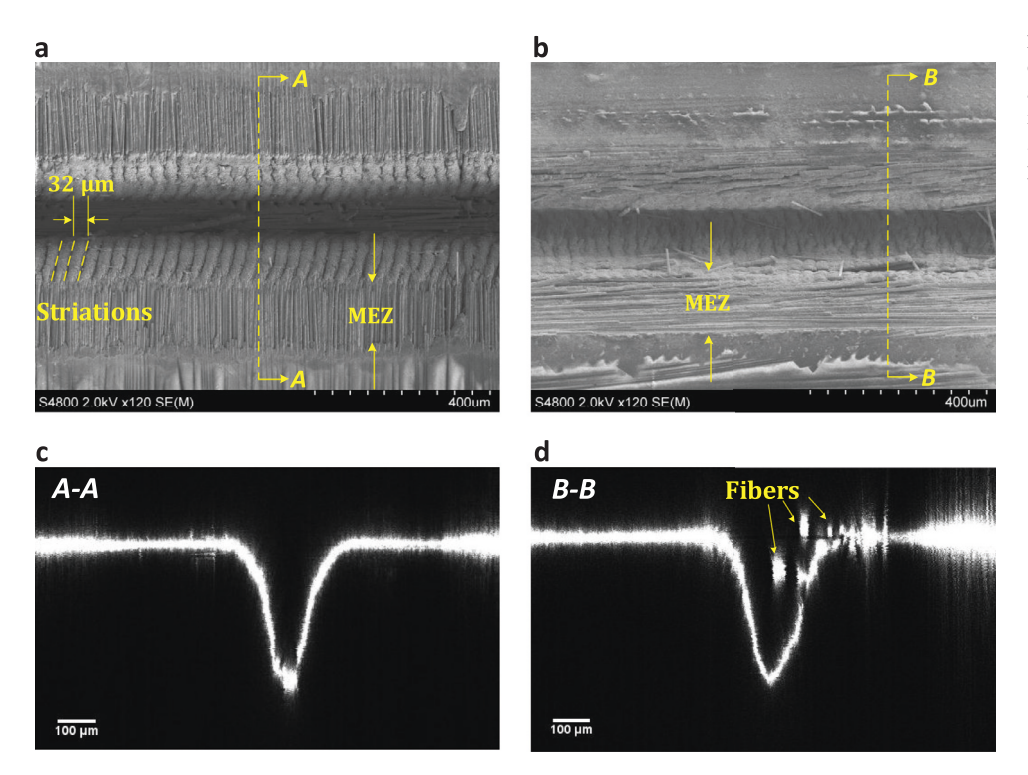


Fig. 4. Micrographs for single-pass laser line cutting of cross-ply IM7 CFRP using LP mode along different direction: (a) SEM micrograph for $\theta = 90^\circ$; (b) SEM micrographs for $\theta = 0^\circ$; (c) 2D confocal profile for $\theta = 90^\circ$; (d) 2D confocal profile for $\theta = 0^\circ$.

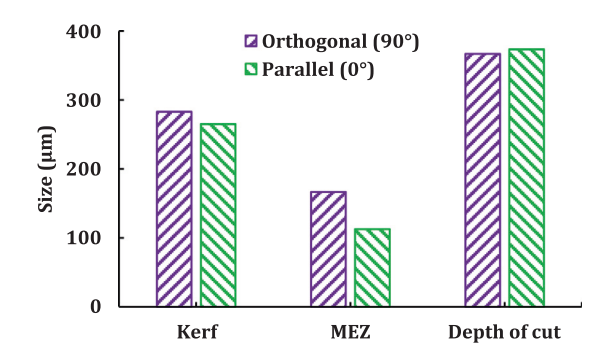


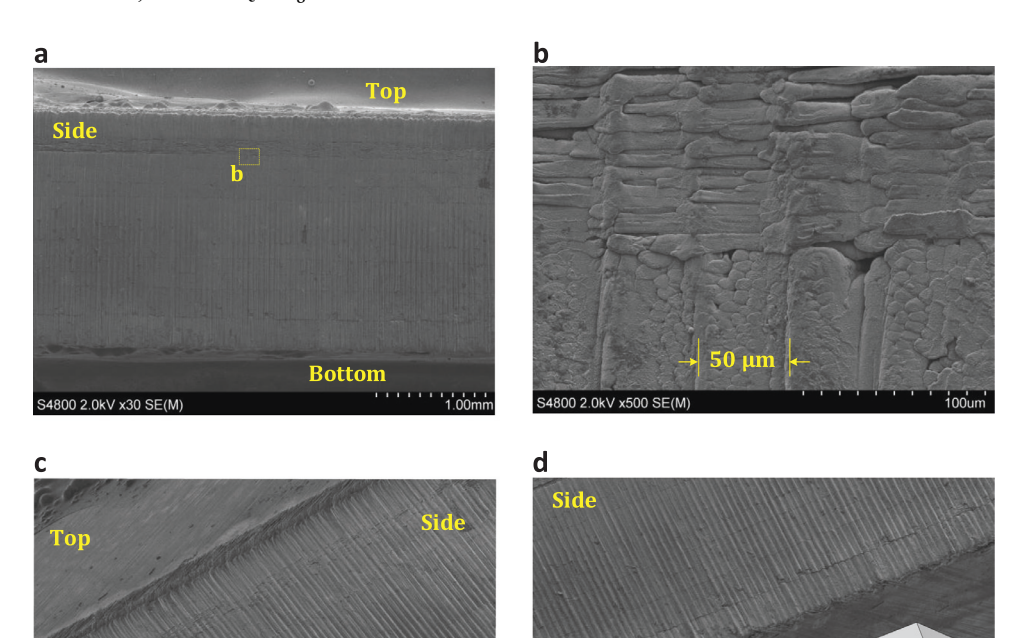
Fig. 5. Machining dimension results from single-pass tests along orthogonal and parallel cutting directions using LP mode.

The mechanism of keyhole cutting of CFRP using a long-duration nanosecond pulse laser is different from that of the CW laser cutting of metal alloys. For the CFRP target, the linear optical absorption coefficient of the polymer matrix is expected to be relatively low. Transmissivity of common matrix materials for CFRP is very high for the wavelength of 1064 nm used in this study. Volkermeyer et al. [34] reported that the transmissivity of Polyamide 6 and Polyphenylene sulfide are about 85%. Similarly, McKie and Addison [35] reported transmissivity of Hercules 3501-5A resin of 93%. Abbas and Ali [36] also showed that the optical absorption coefficient of pure epoxy is very low for 1064 nm wavelengths. Therefore, the laser beam penetrates into a relatively deep region below the CFRP target surface when LP mode is used. Additionally, this means a significant portion of the laser energy is transmitted through the matrix to be directly absorbed and conducted by the carbon fibers. As a result, the high-energy laser beam could be absorbed by a relatively thick layer of the target material to extend the depth of cut. Much of the laser energy is absorbed along the depth by the carbon fibers, which have high absorptivity for 1064 nm wavelengths. The fibers conduct the absorbed energy to the surrounding matrix material, which heats and melts the matrix to form a thin molten material film that allows keyhole formation. The absorbed laser energy may elevate the target material temperature, cause phase transformations, induce material removal from the target, and produce a relatively large cutting depth. Therefore, a new type of keyhole laser cutting using high pulse energy is achieved for CFRP using the long-duration nanosecond pulse laser. It should be noted that future work may still be needed to further verify the above hypothesized explanation and also check whether or not other mechanism(s) has also played an important role.

3.2. Effect of energy density

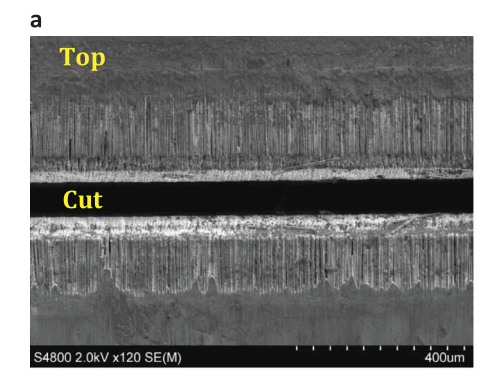
By comparison, woven AS4 CFRP shows a significantly shallower depth of cut and slightly narrower kerf than cross-ply CFRP over the range of tested energy density. This difference was mainly attributed to different fiber layouts and thermal properties. The woven fiber layout leads to more efficient heat transfer along all directions and might affect the penetration depth of laser irradiation into the CFRP material, given the complex reflective properties within the CFRP microstructure [37]. Also, the specific heat of AS4 fibers, 1130 J/kg·K, is almost 30% higher than that of IM7 fibers, 879 J/kg·K. This is reflected in the estimates for critical energy density of approximately 0.79 J/mm² and 2.35 J/mm² for IM7 and AS4 fibers, respectively, which are similar to estimates in [23]. Critical energy density is defined as the minimum energy absorption required for CFRP material removal. Hence, woven AS4 CFRP required more energy input to reach sublimation temperature for photo-thermal laser ablation.

One important takeaway from Fig. 3 is the relationship between laser energy density and machining performance. During the ignition stage in the laser ablation process, a plasma plume consisting of ionized CFRP material expands outward from the target area [38]. This plasma intensifies with laser irradiance, becoming increasingly absorptive of the incoming laser beam. The laser energy that reaches the CFRP surface is reduced in LP mode by the same Bremsstrahlung mechanism as optical breakdown in QSW mode. This process is commonly referred to as plasma shielding. As a result, the ablation rate is also reduced until a saturation level is reached, whereby increasing laser irradiance does not result in more CFRP being removed. This is evidenced by the logarithmic



Bottom
4800 2 0kV v40 SE/M

Fig. 6. SEM micrographs of the side wall surface of a through cut: (a) side wall surface; (b) detailed view at side wall; (c) edge with top surface; (d) edge with bottom surface.



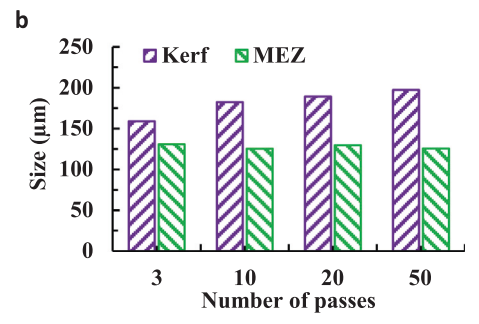


Fig. 7. Effect of pass number in multi-pass laser cutting: (a) SEM micrograph of the top surface after 50 passes; (b) the comparison of kerf and MEZ width after different pass numbers.

trends observed in Fig. 3, particularly for cutting depth. More specifically, for each subsequent laser pass, less CFRP material was removed. The rate by which the cutting depth was increasing began to decrease

over time. The ablation rate is defined by the mass of material removed from the substrate per laser pulse. According to Zeng et al. [39], plasma shielding can be avoided by using pulse durations in the picosecond or femtosecond domain, where ultrashort pulses are fully absorbed by the target material prior to plasma formation.

3.3. Effect of cutting orientation

Bottom

For cross-ply CFRP, the effect of cutting direction relative to the fiber orientation in the top layer was evaluated for parallel ($\theta = 0^{\circ}$) and orthogonal ($\theta = 90^{\circ}$) conditions. The same process parameters were applied for both conditions: beam spot size of 200 µm, energy density of 16.3 J/mm², power intensity of 2.8×10⁹ W/cm², and overlap ratio of 25%. As shown in Fig. 4a, a single-pass laser scan produced a clean and deep cut for $\theta = 90^{\circ}$. Matrix recession was very apparent with large areas of exposed fibers at the top surface, since the heat was conducted away from the target area into the bulk material and increasing the HAZ width. Clear striations along the depth direction can be observed along the trench wall. The spacing between striations was about 32.2 µm, which is nearly equivalent to the theoretic value of the laser feed rate of 32 µm/pulse under scanning speed of 0.32 mm/s and repetition rate of 10 Hz. On the bottom of the trench, fibers parallel to the cutting direction can be observed, which are located in deeper cross-ply laminate layers with different fiber orientation. As shown in Fig. 4b, a single-pass laser scan produced a straight and deep cut for $\theta = 0^{\circ}$. Very little matrix recession can be observed, since heat was conducted along the scanning path. Striations were still noticeable with similar feed mark spacing, but were not as defined as those for $\theta = 90^{\circ}$. Some fiber debris can be observed on the bottom of the trench, and some uncut fibers were exposed along the top edge with a swelled fiber end morphology, likely due to preferential conduction along the fiber axis, which is aligned with the laser scanning path for $\theta = 0^{\circ}$. Fig. 4c-d shows the 2D profiles of the trench cut along directions of 90° and 0°, respectively. The depth of cut was mainly unaffected by cutting direction, but the profile shape was

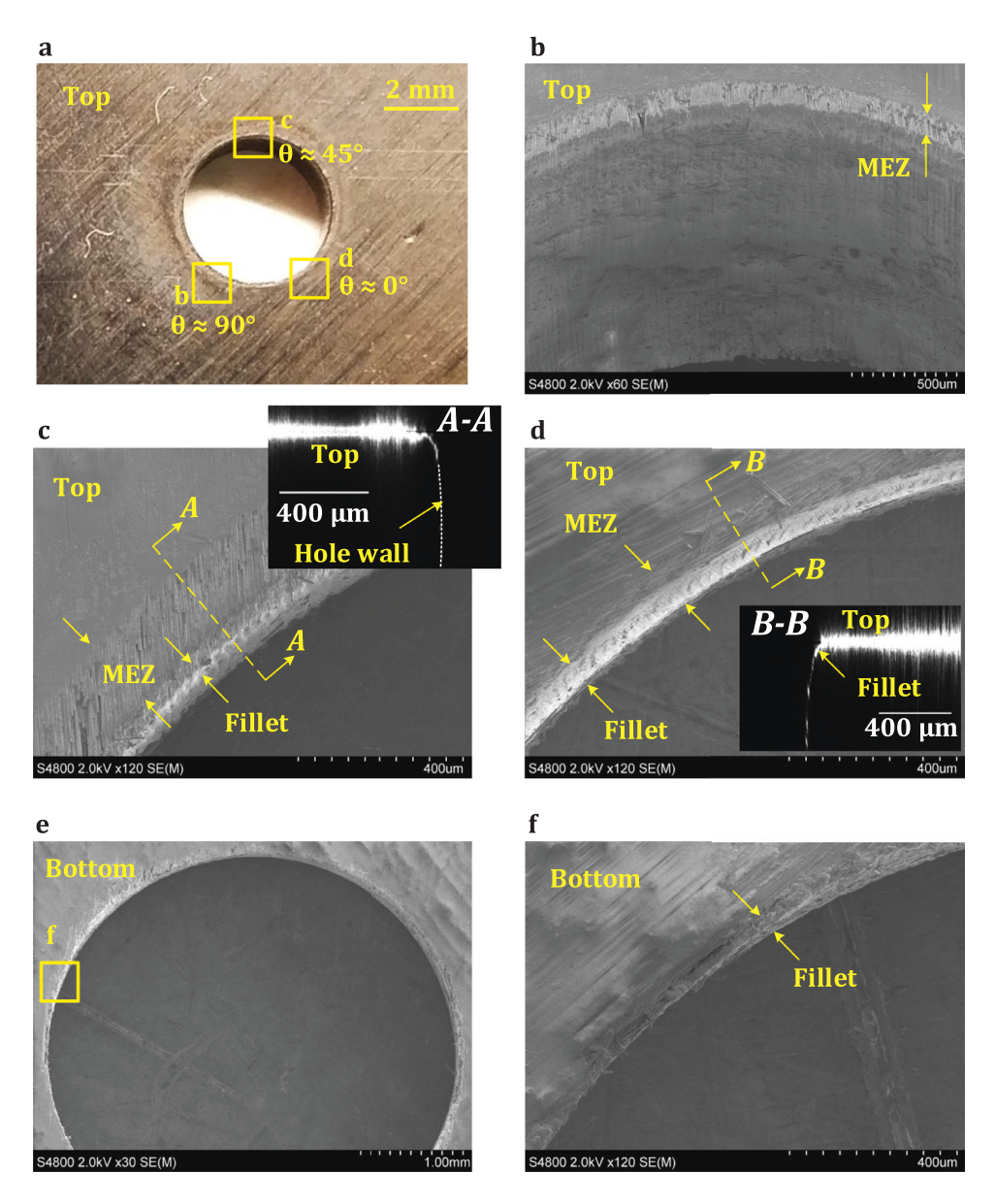


Fig. 8. Contour cutting of cross-ply CFRP using LP mode: (a) entrance of a laser cut round hole with a diameter of 4 mm; (b) SEM image of the edge of hole entrance ($\theta \approx 90^{\circ}$); (c) micrographs of the edge of hole entrance ($\theta \approx 45^{\circ}$); (d) micrographs of the edge of hole entrance ($\theta \approx 0^{\circ}$); (e) exit of a laser cut round hole with a diameter of 4 mm; (f) SEM micrograph of the edge of hole exit ($\theta \approx 0^{\circ}$).

slightly altered. As shown in Fig. 4c, a keyhole shaped profile can be observed for $\theta=90^\circ$, which was enhanced by the slightly wider kerf width in the top layer. Also, the clean profile verified the clean cut characterized using SEM as shown in Fig. 4a. Fig. 4d shows the keyhole shape was not as clear as that for $\theta=90^\circ$ with a slightly tapered profile. The white spots in the 2D profile correspond to the exposed uncut fibers, or fiber pull-out, characterized using SEM as shown in Fig. 4b. In these areas, fibers have absorbed and conducted sufficient energy to induce evaporation of the surrounding matrix, but did not absorb to the point of sublimation. Fig. 5 shows the comparison of the machining dimension along both orthogonal and parallel cutting directions. The MEZ for $\theta=90^\circ$ was about 32% wider than that for $\theta=0^\circ$, whereas the kerf and depth of cut were similar for both cutting directions.

3.4. Machined surface integrity

The machined surface integrity was investigated for multi-pass line through cuts of a 2.2 mm thick cross-ply CFRP panel using SEM shown in Fig. 6. A line cut was machined using the spot size of $100 \, \mu m$, energy density of $54 \, J/mm^2$, power intensity of $2.9 \times 10^{10} \, W/cm^2$, and overlap ratio of 40%. Optical breakdown is avoided due to the longer 120 ns

pulse duration, despite power intensity exceeding the theoretical threshold for QSW discussed in Section 3.1. Under these conditions, a 2.2 mm thick cross-ply CFRP panel was cut through as few as 6 passes. Fig. 6a shows a high quality side surface of a cut where the horizontal striations indicate the boundary between different laminate layers. This is shown in Fig. 6b shows a detailed view of the side wall, where two laminates with different fiber orientations are illustrated. The fiber direction in the top layer was parallel to the laser scan direction ($\theta = 0^{\circ}$), whereas the next layer was perpendicular to the laser scan direction $(\theta = 90^{\circ})$. No fiber pull-out is observed on the side wall surface with limited fiber swelling. The spacing between two adjacent striations was measured as $50\,\mu m$, which is consistent with the laser feed rate for a scanning speed of 0.5 mm/s and repetition rate of 10 Hz. Fig. 6c-d show sharp edges with limited MEZ formation at the top and bottom surfaces, respectively. These surface morphology analyses demonstrate the high quality and efficiency of line cutting of CFRP panels by keyhole mode material removal LP mode.

Striations are often observed on the machined surface for laser cutting of metal alloys. Arata et al. [40] suggested that lateral-burning exothermic reactions between oxygen and iron were the main cause of striation formation for ${\rm CO}_2$ laser cutting of mild steels. However, stri-

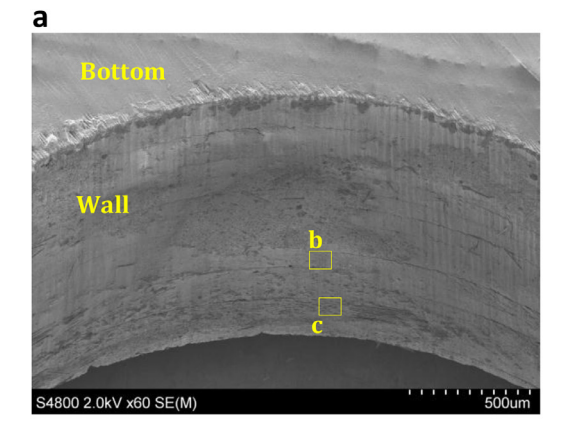
ations are widely observed during laser cutting of metal alloys and ceramics when no oxidation takes place with the use of inert gases such as nitrogen and argon [41,42]. Chen and Yao [43] developed a more comprehensive theory based on the instability of a thin liquid film in a high-velocity gas jet and diffusion-controlled oxidation to explain the formation of striations during laser cutting. In thin-section steel, these striations are usually clear and straight from the top of the cut edge to the bottom. However, for thick panels, striations are replaced by random ripples or drag lines near the bottom, which are associated with the flow of liquid out of the cut zone [44].

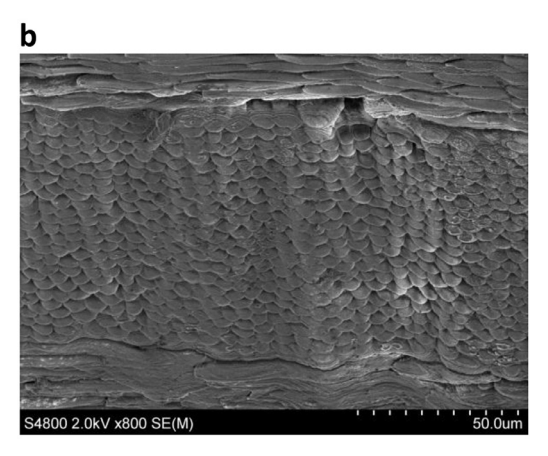
SEM micrographs in this study show that all the striations are straight and uniformly distributed throughout the whole CFRP specimen thickness. The striations on the machined CFRP surface result from the last laser scan from the multi-pass keyhole laser cutting process, with the measured spacing between adjacent striations being equivalent to the spacing of two subsequent laser pulses, as shown in Fig. 4a and Fig. 6b. This might be from the reduced volume of molten material present during CFRP laser cutting. CFRP fibers sublimate directly from solid to gas phase while the matrix experiences melting prior to evaporation. Given a fiber volume fraction of 57% or 62%, it is hypothesized that only a small portion of the remaining matrix forms a liquid material volume during the laser absorption process. Therefore, the mechanism of striations of this keyhole laser cutting CFRP process is different from conventional laser cutting of metal alloys.

The effect of scan pass number on the scanned top surface was evaluated under a moderate energy density of $31\,\mathrm{J/mm^2}.$ The other process parameters were spot size of $100\,\mu m$, power intensity of $1.1\times10^{10}\,\mathrm{W/cm^2},$ and overlap ratio of 60%. Fig. 7a shows the SEM graph of a typical cut after 50 passes. A clean cut was obtained with the kerf width of 198 μm and MEZ width of 126 μm at the entrance. Fig. 7b shows the comparison of the kerf and MEZ under different scan passes. It can be seen that the kerf width was increased with the number of passes until 10 until becoming saturated, which can be explained by laser shadowing of a Gaussian beam. However, the MEZ width was mainly unaffected by the increase of pass number, which indicated that no more thermal damage would be further introduced by the increase of laser scan passes.

3.5. Contour cutting experiment

Circular holes of 4 mm and 6 mm diameter were obtained in contour cutting experiments. Fig. 8a shows the top view of a circular hole with the diameter of 4 mm using a beam spot size of 75 µm, energy density of 116.9 J/mm², power intensity of 5.0×10^{10} W/cm², and overlap ratio of 47%. Fig. 8b, c, and d show the top surface near the hole entrance edge and the 2D surface profile where the cutting direction was approximately 90° perpendicular, 45° relative, and 0° parallel to the fiber orientation in the top layer, respectively. The heat-affected zone, especially for MEZ, was found to be non-uniform around the hole circumference, as expected given the results from Section 3.3. As shown in Fig. 8b, a MEZ ring can be seen outside the hole entrance edge, which was about 164 µm wide. As shown in Fig. 8c, the width of MEZ was decreased slightly for 45°. Lastly in Fig. 8d, the MEZ width was reduced to a minimal level when the cutting direction was parallel to the local fiber orientation in the top layer. The width of MEZ depended on the relative direction between laser cutting and fiber orientation. The variation of the MEZ width should be a result of the different thermal conductivity along the fiber direction or across the fiber direction in the CFRP panel. A fillet was formed along the hole entrance edge as shown in the 2D profile near the hole entrance. The formation of the fillet was attributed to the wider kerf on the top surface, which was similar to the line cutting results from Section 3.1. Due to the almost vertical hole internal wall surface, high gain was used during the confocal microscopy, which caused the high noise on the top surface. These fillet domains correspond to a narrow ring area between the MEZ and hole surface, which are shown in the SEM micrographs. This fillet cannot be observed along





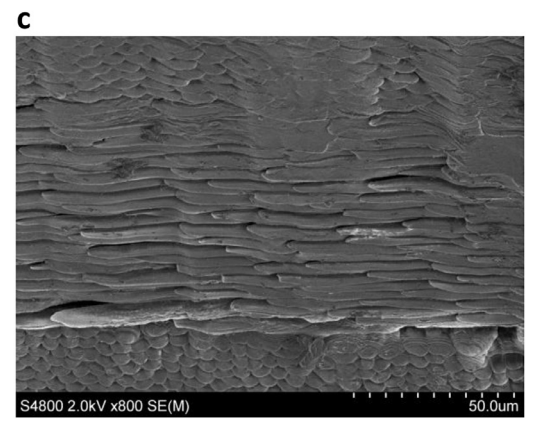


Fig. 9. SEM micrograph wall surface of the hole: (a) the wall surface from the exit; (b) the detailed view on wall surface ($\theta \approx 90^{\circ}$); (c) the detailed view on the wall surface ($\theta \approx 0^{\circ}$).

the hole exit edge. As shown in Fig. 8e and f, a sharp edge can be observed along the hole exit. The MEZ shown in Fig. 8f was very minimal in this SEM micrograph since the cutting direction was nearly parallel to the fiber orientation in the bottom layer.

The wall surface of the circular hole was characterized in Fig. 9. As shown in Fig. 9a, a smooth texture was obtained on the hole surface, and a sharp edge can be observed between the hole surface and bottom surface. Similar to the side surface of a line cut shown in Fig. 6 of Section 3.4, the vertical striations can be observed through the CFRP panel thickness, and the horizontal marks of different laminates can be observed. Fig. 9b and c show the detailed view at the laminates with fiber direction perpendicular and parallel to the cutting direction, respectively. No fiber pull-out can be observed on the hole surface, and only limited fiber swelling can be observed at the end of fibers.

4. Conclusion

This experimental study demonstrates for the first time that keyhole mode cutting can be achieved for CFRP materials by a high-energy nanosecond pulse laser using LP mode. The formation of keyhole-shaped trench is attributed to laser ablation of the carbon fibers and conduction to the polymer matrix to create a small molten material volume, allowing deep penetration of laser energy for increased cutting efficiency compared with low energy nanosecond lasers. It is also shown that the shortduration QSW mode results in ineffective cutting performance for CFRP because of nonlinear optical absorption and subsequent Bremsstrahlung absorption by laser-induced plasma due to high power intensity above threshold values. Under LP mode, a single-pass laser scan can produce a clean and deep trench profile with a clear keyhole shape, while a 6pass laser process can cut through a 2.2 mm thick cross-ply CFRP panel, indicating a much higher ablation rate than low-energy, high-frequency laser. Laser energy density was compared to power intensity as a control variable, with minimal energy input values closely matching values from other researchers. The effects of laser shielding were observed by decreasing ablation efficiency for increasing energy density.

A high-quality machined surface can be produced with a limited heat-affected zone and little fiber pull-out using inert Argon assist gas, with a slight dependence on fiber orientation relative to the cutting direction. Uniform striations on the machined surface result from the last laser pass of the multi-pass cutting process according to the laser feed rate, and form by a proposed different mechanism than during conventional laser cutting of metal alloys. These experiments highlight the advantages of high-energy ns-pulsing in CFRP laser machining, while exploring associated limitations. The successful outcomes from this work provide the key to enable an efficient high-quality laser machining process for CFRP materials.

Acknowledgements

The authors gratefully acknowledge the financial support by the National Science Foundation under Grant Number CMMI-1537512.

Supplementary material

Supplementary material associated with this article can be found, in the online version, at doi:10.1016/j.optlaseng.2019.03.009.

References

- Salama A, Li L, Mativenga P, Sabli A. High-power picosecond laser drilling/machining of carbon fibre-reinforced polymer (CFRP) composites. Appl Phys A 2016;122:73. doi:10.1007/s00339-016-9607-8.
- [2] Salama A, Li L, Mativenga P, Whitehead D. TEA CO₂ laser machining of CFRP composite. Appl Phys A 2016;122:497. doi:10.1007/s00339-016-0025-8.
- [3] Jung K-W, Kawahito Y, Katayama S. Ultra-high speed disk laser cutting of carbon fiber reinforced plastics. J Laser Appl 2012;24:012007. doi:10.2351/1.3673521.
- [4] Leone C, Papa I, Tagliaferri F, Lopresto V. Investigation of CFRP laser milling using a 30 W Q-switched Yb:YAG fiber laser: effect of process parameters on removal mechanisms and HAZ formation. Compos Part A Appl Sci Manuf 2013;55:129–42. doi:10.1016/j.compositesa.2013.08.004.
- [5] Li ZL, Zheng HY, Lim GC, Chu PL, Li L. Study on UV laser machining quality of carbon fibre reinforced composites. Compos Part A Appl Sci Manuf 2010;41:1403– 8. doi:10.1016/j.compositesa.2010.05.017.
- [6] Mathew J, Goswami GL, Ramakrishnan N, Naik NK. Parametric studies on pulsed Nd:YAG laser cutting of carbon fibre reinforced plastic composites. J Mater Process Technol 1999;89–90:198–203. doi:10.1016/S0924-0136(99)00011-4.
- [7] Anzai K, Aoyama M, Fujisaki A, Miyato T, Kayahara T, Harada Y, et al. Laser trepanning of CFRP with a scanner head for IR and UV lasers. Proc SPIE 2014;8967 89670K–89670K–6. doi:10.1117/12.2037264.
- [8] Fujita M, Ohkawa H, Somekawa T, Otsuka M, Maeda Y, Matsutani T, et al. Wavelength and pulse width dependences of laser processing of CFRP. Phys Procedia 2016;83:1031–6. doi:10.1016/j.phpro.2016.08.108.
- [9] Takahashi K, Tsukamoto M, Masuno S, Sato Y. Heat conduction analysis of laser CFRP processing with IR and UV laser light. Compos Part A Appl Sci Manuf 2016;84:114–22. doi:10.1016/j.compositesa.2015.12.009.
- [10] Wolynski A, Herrmann T, Mucha P, Haloui H, L'huillier J. Laser ablation of CFRP using picosecond laser pulses at different wavelengths from UV to IR. Phys Procedia 2011;12:292–301. doi:10.1016/j.phpro.2011.03.136.

- [11] Voisey KT, Fouquet S, Roy D, Clyne TW. Fibre swelling during laser drilling of carbon fibre composites. Opt Lasers Eng 2006;44:1185–97. doi:10.1016/j.optlaseng.2005.10.008.
- [12] Fuchs AN, Schoeberl M, Tremmer J, Zaeh MF. Laser cutting of carbon fiber fabrics. Phys Procedia 2013;41:372–80. doi:10.1016/j.phpro.2013.03.090.
- [13] Li ZL, Chu P, Zheng H, Lim G, Li L, Marimuthu S, et al. Process development of laser machining of carbon fibre reinfoenced plastic composites. In: 27th Int. Congr. Appl. Lasers Electro-Optics (ICALEO08); 2008. p. 222–30. 20-23 Oct.
- [14] Riveiro A, Quintero F, Lusquiños F, del Val J, Comesaña R, Boutinguiza M, et al. Experimental study on the CO₂ laser cutting of carbon fiber reinforced plastic composite. Compos Part A Appl Sci Manuf 2012;43:1400–9. doi:10.1016/j.compositesa.2012.02.012.
- [15] Rodden WS. A comprehensive study of the long pulse Nd:YAG laser drilling of multi-layer carbon fibre composites. Opt Commun 2002;210:319–28. doi:10.1016/S0030-4018(02)01807-2
- [16] Negarestani R, Li L, Sezer HK, Whitehead D, Methven J. Nano-second pulsed DPSS Nd:YAG laser cutting of CFRP composites with mixed reactive and inert gases. Int J Adv Manuf Technol 2010;49:553–66. doi:10.1007/s00170-009-2431-y.
- [17] French P, Naeem M, Wolynski A, Sharp M. Fibre laser material processing of aerospace composites 2010;103:1028–35.
- [18] Finger J, Weinand M, Wortmann D. Ablation and cutting of carbon-fiber reinforced plastics using picosecond pulsed laser radiation with high average power. J Laser Appl 2013;25:042007. doi:10.2351/1.4807082.
- [19] Loumena C, Nguyen M, Lopez J, Kling R. Potentials for lasers in CFRP production 2018;1026:1026–34. doi:10.2351/1.5062378.
- [20] Hoffman J, Chrzanowska J, Kucharski S, Moscicki T, Mihailescu IN, Ristoscu C, et al. The effect of laser wavelength on the ablation rate of carbon. Appl Phys A 2014;117:395–400.
- [21] Lednev VN, Pershin SM, Obraztsova ED, Kudryashov SI, Bunkin AF. Single-shot and single-spot measurement of laser ablation threshold for carbon nanotubes. J Phys D Appl Phys 2013;46:52002.
- [22] Beal VE, Paggi RA, Salmoria G V. Lago A. Statistical evaluation of laser energy density effect on mechanical properties of polyamide parts manufactured by selective laser sintering. J Appl Polym Sci 2009;113:2910–19. doi:10.1002/app.30329.
- [23] Romoli L, Fischer F, Kling R. A study on UV laser drilling of PEEK reinforced with carbon fibers. Opt Lasers Eng 2012;50:449–57. doi:10.1016/j.optlaseng.2011.10.008.
- [24] Hexcel. HexTow® IM7 2014.
- [25] Hexcel. HexTow® AS4 2014.
- [26] Takahashi K, Tsukamoto M, Masuno S, Sato Y, Yoshida H, Tsubakimoto K, et al. Influence of laser scanning conditions on CFRP processing with a pulsed fiber laser. J Mater Process Technol 2015;222:110–21. doi:10.1016/j.jmatprotec.2015.02.043.
- [27] Sato Y, Tsukamoto M, Matsuoka F, Ohkubo T, Abe N. Thermal effect on CFRP ablation with a 100-W class pulse fiber laser using a PCF amplifier. Appl Surf Sci 2017;417:250–5. doi:10.1016/j.apsusc.2017.03.286.
- [28] Thiyagarajan M, Thompson S. Optical breakdown threshold investigation of 1064 nm laser induced air plasmas. J Appl Phys 2012;111:73302.
- [29] Kroll N, Watson KM. Theoretical study of ionization of air by intense laser pulses. Phys Rev A 1972;5:1883–905. doi:10.1103/PhysRevA.5.1883.
- [30] Sankaranarayanan S, Kar A. Nonlinear effects of laser-plasma interaction on melt-surface temperature. J Phys D Appl Phys 1999;32:777–84. doi:10.1088/0022-3727/32/7/005.
- [31] Morgan CG. Laser-induced breakdown of gases. Rep Prog Phys 1975;38:621–65. doi:10.1088/0034-4885/38/5/002.
- [32] Wu CW, Wu XQ, Huang CG. Ablation behaviors of carbon reinforced polymer composites by laser of different operation modes. Opt Laser Technol 2015;73:23–8. doi:10.1016/j.optlastec.2015.04.008.
- [33] Preissig K-U, Petring D, Herziger G. High-speed laser cutting of thin metal sheets. In: Beyer E, Cantello M, La Rocca A V., Laude LD, Olsen FO, Sepold G, editors., 1994, p. 96. doi:10.1117/12.184714.
- [34] Völkermeyer F, Fischer F, Stute U, Kracht D. Laser-based approach for bonded repair of carbon fiber reinforced plastics. Phys Procedia 2011;12:537–42. doi:10.1016/j.phpro.2011.03.066.
- [35] McKie ADW, Addison RC. Practical considerations for the rapid inspection of composite materials using laser-based ultrasound. Ultrasonics 1994;32:333–45. doi:10.1016/0041-624X(94)90103-1.
- [36] Abbas FS, Ali NF. Study the optical characteristics of epoxy panel doped with fluorescein-sodium dye. J Kerbala Univ 2014;12:50–60.
- [37] Xu H, Hu J, Yu Z. Absorption behavior analysis of carbon fiber reinforced polymer in laser processing. Opt Mater Express 2015;5:2330. doi:10.1364/OME.5.002330.
- [38] Russo RE, Mao XL, Yoo JH, Gonzalez JJ. Laser ablation. Laser-induced break, 978-044451734-0. Spectrosc; 2007. p. 49–82. doi:10.1016/B.50006-5.
- [39] Zeng X, Mao XL, Greif R, Russo RE. Experimental investigation of ablation efficiency and plasma expansion during femtosecond and nanosecond laser ablation of silicon. Appl Phys A Mater Sci Process 2005;80:237–41.
- [40] Arata Y, Maruo H, Miyamoto I, Takeuchi S. Dynamic behavior in laser gas cutting of Mild steel (welding physics, processes & instruments) 1979.
- [41] Ivarson A, Powell J, Kamalu J, Magnusson C. The oxidation dynamics of laser cutting of mild steel and the generation of striations on the cut edge. J Mater Process Technol 1994;40:359–74. doi:10.1016/0924-0136(94)90461-8.
- [42] Li L, Sobih M, Crouse PL. Striation-free laser cutting of mild steel sheets. CIRP Ann - Manuf Technol 2007;56:193–6. doi:10.1016/j.cirp.2007.05.047.
- [43] Chen K, Yao LY. Striation formation and melt removal in the laser cutting process. J Manuf Process 1999:1:43–53. doi:10.1016/S1526-6125(99)70004-6.
- [44] Powell J. Laser cutting steels. $\rm CO_2$ laser cut. London: Springer London; 1993. p. 23–70. doi:10.1007/978-1-4471-3384-1_2.